ACS APPLIED MATERIALS & INTERFACES

Research Article

www.acsami.org

Profile Control of Inkjet Printed Silver Electrodes and Their Application to Organic Transistors

Kenjiro Fukuda,* Tomohito Sekine, Daisuke Kumaki, and Shizuo Tokito*

Graduate School of Science and Engineering and Research Center for Organic Electronics (ROEL), Yamagata University, 4-3-16 Jonan, Yonezawa, Yamagata, 992-8510, Japan

ABSTRACT: We report on the cross-sectional profile control of printed electrodes fabricated from silver nanoparticle inks with water-based solvents by inkjet printing. Systematically varying the ambient conditions and time for the drying process corresponded to changes in electrode shape. In general, lower humidity levels resulted in concave electrode profiles due to the coffee-ring effect, while higher humidity levels resulted in convex profiles. Printed capacitors with trapezoidal-shaped lower electrodes showed much better electrical breakdown strength than those with concave-shaped lower electrodes. Solution-processed organic thin-film transistors with trapezoidal gate electrodes operated reproducibly and exhibited good electrical characteristics with very low gate-leakage currents. The methods can be utilized in the fabrication of printed electronic devices with stacked layers, such as thin-film capacitors and transistors.

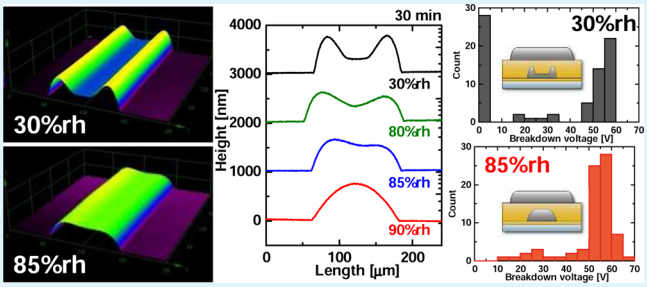

KEYWORDS: *inkjet printing, silver nanoparticle ink, profile control, organic thin-film transistors, printed electronics, humidity*

INTRODUCTION

Printed electronics technology has attracted significant attention in recent years because fabrication processes based on printing have a number of advantages over conventional photolithography. Printable processes can dramatically reduce material waste and manufacturing process steps, while lowering manufacturing costs. Moreover, they can be readily scaled to large-area production with high throughput. These features enable low-cost, large-area flexible device applications, which lead to new ways to develop electronics in areas such as organic light-emitting-diodes,[1] organic solar cells,[2] thin-film transistors,[3−5] logic circuits,[6] radio frequency identification (RFID) tags,[7,8] sensors,[9,10] and detectors.[11]

When printed ink dries on the surface of a substrate, the solute is generally transported from the center to the edge, and the resulting solute film forms a nonuniform ringlike profile. Deegan et al. studied this phenomenon, known as the "coffee-ring effect", for colloidal suspension systems.[12] The nonuniform profile in the cross-section for printed electrodes originating from this effect is the major issue to be solved for the devices with stacked layers such as capacitors and thin-film transistors (TFTs). The thicker edges of lower electrodes interfere with the flatness and uniformity of overlying dielectric layers. As a result, fully solution processed TFT devices have difficulty operating at high voltages due to the potential for electrical shorts between the lower and upper electrodes.[13,14] Several approaches have been proposed to suppress the nonuniformities in printed films, such as controlling of the initial contact angle of the droplet,[15] use of a mixed solvent,[16,17] the addition of small amount of surfactants,[18,19] changing the surface temperature,[20−22] optimizing the drying temperature,[23] using solvent vapor atmosphere,[24,25] employing hydrosoluble polymer additives during droplet evaporation,[26] and using ellipsoidal particles for the solute.[27] In this study, we have focused on the inkjet printed metal nanoparticles as currently used for electrode materials in printed electronic devices.[28−32] We report on inkjet-printed silver electrodes whose cross-sectional shape is controlled by changing the drying conditions, namely the ambient humidity and drying time. Here, we used silver nanoparticles dispersed in a water-based solvent. Ideal electrodes with flat and trapezoidal shapes were obtained at 85% relative humidity (RH) for 30 min. The capacitor and organic thin-film transistor devices formed with the flat, trapezoidal lower electrodes showed excellent durability during operation.

EXPERIMENTAL SECTION

Materials. Cross-linked poly-4-vinylphenol (PVP) was used as a base layer for controlling the surface energy of the glass substrate. PVP (M_w ~ 25 000, Sigma Aldrich Co.) and poly(melamine-co-formaldehyde) (M_n ~ 432, 84 wt %, Sigma Aldrich Co.) as a cross-linking agent were mixed in propylene glycol monomethyl ether acetate (PGMEA). The PVP solution was spin-coated onto glass substrates and was thermally cross-linked at temperatures of 150 °C for 60 min to form a base layer.

Inkjet Printing and Drying Condition. The silver ink used in this work was based on silver nanoparticles in a water-based solvent

Received: February 19, 2013
Accepted: April 2, 2013
Published: April 2, 2013

(JAGLT Series, DIC, Corp. Japan). This ink contained 25−35 wt % silver nanoparticles with an average diameter of 20−40 nm. The silver nanoparticle ink was patterned with an inkjet printer (Fujifilm Dimatix, DMP2800) onto the cross-linked PVP layers using a print head with 10 pL nozzles. The silver nanoparticle ink was printed using a customized waveform. The droplets were deposited with a dot-to-dot spacing of 20 μm and resulted in printed lines of length 15 mm. During the inkjet patterning process, the substrate temperature was maintained at 30 °C.

After the printing, the substrates were maintained at 30 °C, 30% RH for 5 min and then stored in an environmental test chamber following the printing process (espec, SH-221) in order to evaporate the solvents from printed ink. Temperature in the chamber was held at 30 °C, and relative humidity was changed from 30% to 90%, while the storage time was also varied from 5 to 45 min. After the drying process, the substrates were heated at 140 °C for 1 h to sinter the silver nanoparticles.

Fabrication Process of Thin-Film Capacitors and Organic Thin-Film Transistor Devices. To investigate how the flatness of the electrodes affected the functionality and performance of electronic devices with stacked layer constructions, thin-film capacitors and organic TFT devices were fabricated. Two types of silver layers with different drying conditions were prepared as gate electrodes: (i) 30 °C, 30% RH for 30 min and (ii) 30 °C, 85% RH for 30 min. After forming these electrodes, a solution of cross-linked PVP was spin-coated and baked to form 210-nm thick dielectric layers. Silver nanoparticle ink was then applied using inkjet printing to form the upper source/drain electrodes. To fabricate the organic TFT devices, a 50-nm pentacene semiconducting layer was also deposited.

Characterization. The silver electrode profiles were measured using laser micrograph (Olympus, OLS 4200), whereby we assessed the dependencies the ambient humidity and drying time on the profiles. In order to investigate how ambient humidity affects the nanoscale morphology of the printed silver electrodes, the printed lines were examined by scanning electron microscope (SEM; JEOL, JSM-7600FA). The resistivity of printed lines and electrical characteristics for the fabricated capacitors and TFT devices were measured by using a semiconductor parameter analyzer (Keithley, 4200-SCS). All measurements were made after a 140 °C sintering process. All electrical measurements of organic TFT devices were were performed in a nitrogen atmosphere to prevent degradation of organic semiconductors induced by oxygen or moisture.[33,34]

RESULTS AND DISCUSSION

Figures 1a and b show line profiles (cross-sectional and 3D views) of printed silver electrodes dried at various humidity levels. The drying time in the environmental test chamber was 30 min for each of the electrodes. The electrode profiles varied widely with the ambient humidity in the chamber. The cross-sectional profile for a line with ambient humidity of 30% RH was concave. These nonuniformities in silver electrode thickness are a result of the coffee-ring effect. The ratio of thickness between the edge and center of the profile (t_e/t_c) is 3.0. This concave shape was suppressed by increasing the ambient humidity from 30% to 80% RH (t_e/t_c = 2.1), such that a nearly trapezoidal shape was observed at an ambient humidity level of 85% RH (t_e/t_c = 1.3). Furthermore, for ambient humidity levels of 90% RH the silver electrodes formed a convex shape (t_e/t_c < 1). These results clearly show that the silver electrode profiles were very sensitive to the ambient humidity levels during the drying process. Additionally, the cross-sectional areas of the profiles were nearly the same and within a range of 56−63 μm^2, which indicated that increasing ambient humidity did not affect the density of the silver in the electrode layers. The silver electrode resistivity obtained as a function of ambient humidity is shown in Figure 1c. The resistivity decreased from 40 to 27 $\mu\Omega$ cm as the relative

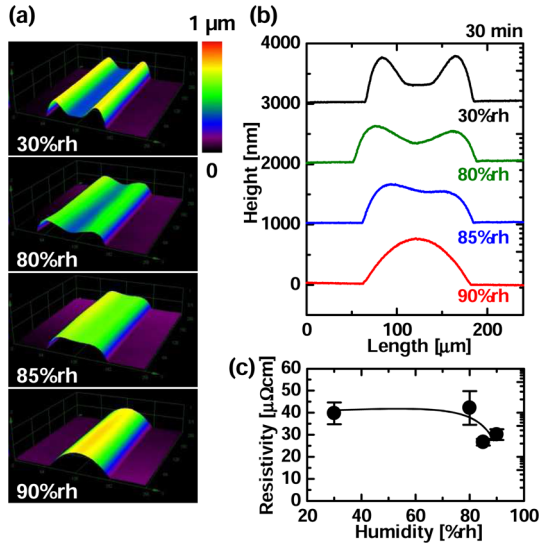

Figure 1. Controlling the shape of inkjet printed silver electrodes by changing the ambient humidity. The temperature of the chamber and drying time were 30 °C and 30 min. All the measurements were made after a 140 °C sintering process. (a) Laser microscopic images of the electrodes for 30%, 80%, 85%, and 90% RH. (b) Profiles for the same electrodes. (c) Resistivity values of the resulting silver electrodes as a function of ambient humidity.

humidity increased from 30% to 85% RH, which demonstrated that electrodes with uniform profiles have better conductivity than those with nonuniform profiles. Several groups have reported that concave-shaped ridged profiles exhibit low conductivity even after heat treament.[17,21] These resistivity results in this study agree with these previous reports.

The dependence of drying time on the electrode profiles was also assessed. Figure 2a and b shows variations of the line profiles (cross-sectional and 3D views) vs drying time. The relative humidity in the chamber was held at 90% for all electrodes. Even for short drying times of 5 min, the silver electrode profiles became increasingly flatter (t_e/t_c = 1.6). For drying times of 10 min, the layer profiles were almost completely flat (t_e/t_c = 1.1). In further extending the drying time to 15 min, the profiles became convex, and line profiles in RH 90% ambient were nearly unchanged for exposure times over 15 min. The resistivity of obtained silver electrodes as a function of drying time in the chamber with elevated humidity levels is shown in Figure 2c. The resistivities for these electrodes were almost the same even though the drying time was varied from 5 to 45 min, and they showed lower resistivities than those dried in low-humidity conditions. While the electrodes with drying times of 5 min have concave shape, the resistivities of those lines were relatively low compared to other concave lines. This was attributed to a reduction in the thickness ratio between the edge and center of the profile.

In order to the characterize the line profile control mechanism by changing the relative humidity, we consider the evaporation rate of the solvent.[35,36] In our experiments, evaporation occurs in a quasi-steady manner because the diffusion time for water vapor in air is much smaller than the evaporation time. The concentration field around the printed line is given by

$$\Delta c = 0 \quad (1)$$

dx.doi.org/10.1021/am400632s | ACS Appl. Mater. Interfaces 2013, 5, 3916−3920

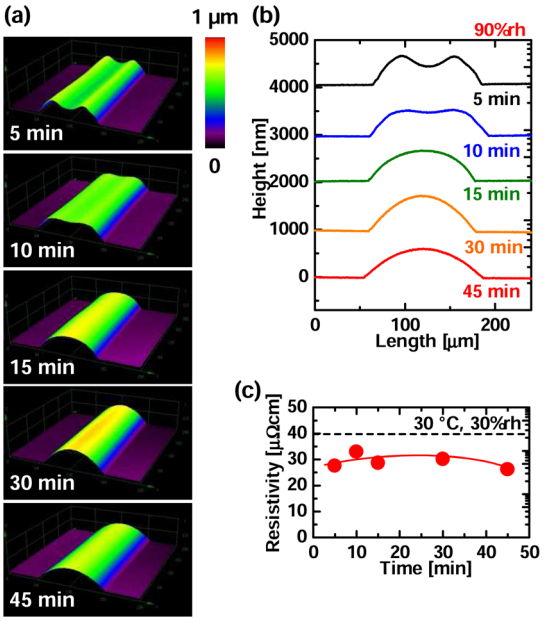

Figure 2. Controlling the shape of inkjet printed silver electrodes by changing the drying time with controlled temperature and humidity. The temperature and humidity in the chamber were 30 °C and 90% RH. All the measurements were made after a 140 °C sintering process. (a) Laser microscopic images of the electrodes of for drying times of 5, 10, 15, 30, and 45 min. (b) Profiles for the same electrodes. (c) Resistivity values of the resulting silver electrodes as a function of storage time.

where c is the local water vapor mass concentration. At the interface between the liquid and vapor, the vapor concentration c is assumed to equal the saturation value c_v. Far above the droplet, the vapor concentration approaches an ambient value $H_{c,v}$ where H is the relative humidity of the ambient air. The difference in water vapor concentration $c_v(1 - H)$ drives the evaporation into air. The diffusive flux is given by Fick's law:

$$J_s = -D_s \nabla c \quad (2)$$

where J_s is the solvent evaporation rate and D_s is the vapor diffusivity. This equation indicates that higher humidity levels cause a reduction in evaporation rate for aqueous solvents. Okuzono et al. have proposed a simple model that predicts a final shape of a dried thin film.[37] According to the model, J_s and diffusion coefficient (D) affect the final shape of the film. The smaller the value of J_s or the larger the value D, the more readily a convex shape is formed. This is because diffusion tends to homogenize the concentration field contrary to the outward flow. In this study, humidity level did not affect D but did affect J_s. At higher humidity levels, diffusion became dominant during the drying process, which caused the silver electrode shapes to change from concave to convex. Indeed, a dependence of electrode shape on ambient humidity was not observed in the electrodes obtained from silver nanoparticle inks dispersed in hydrocarbon solvents because the humidity level did not affect the evaporation rate of the solvents. Aqueous solvents facilitate control of the electrode shape through changes in ambient humidity, without changing other key parameters, such as electrode resistivity and line width.

Furthermore, the results for the dependence on drying time as shown in Figure 2 indicate that the final shape of thin films can be best controlled by combining partial drying with high ambient humidity levels and rapid evaporation at high temperatures. Because of shortened drying times at high ambient humidity levels, the solvents were not completely evaporated from the films, whereby the solvent was further evaporated during the sintering process at 140 °C.

In order to investigate how ambient humidity affects the nanoscale morphology of the printed silver electrodes, we observed the printed silver electrodes with a scanning electron microscope (SEM; JEOL, JSM-7600FA). Figure 3 shows

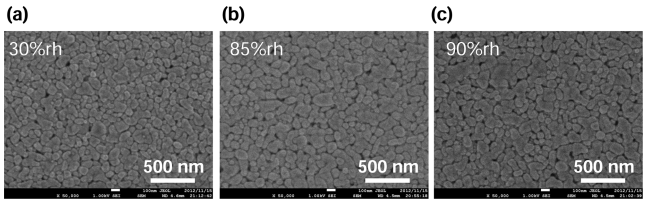

Figure 3. SEM images of formed silver electrodes on the substrates with storage humidity of (a) 30%, (b) 85%, and (c) 90% RH. All of the electrodes were sintered at 140 °C after storage in the controlled ambient environment.

surface images at the center of the silver electrode layers prepared at different drying conditions. All images show dense layers with closely packed silver grains with an average diameter of 100 nm. These images indicate that, even though ambient humidity affects the macroscopic profiles, it does not affect film morphology.

Figure 4a and b shows histograms for the electrical breakdown voltage results of the fabricated capacitors with two different lower silver electrodes prepared at drying conditions of 30 °C, 30% RH for 30 min (a) and 30 °C, 85% RH for 30 min (b). The capacitors with concave shaped electrodes did not have sufficient insulating properties; 37% of the capacitors exhibited a breakdown voltage of less than 5 V, as shown in Figure 4a, which indicates that the upper and lower electrodes had shorted. The peaks of the lower electrodes pose nonuniformity of the dielectric layers and/or the increase of the electric field at the edge of the lower electrodes, which causes the shorted capacitors. On the other hand, no capacitor electrodes shorted when the trapezoidal shaped electrodes were used for the lower electrodes. Additionally, the average breakdown voltage improved from 33 to 52 V by using trapezoidal shaped electrodes. A breakdown voltage of 52 V corresponds to 2.54 MV/cm in electric field strength, which was comparable to that for cross-linked PVP used as dielectric layers and evaporated metal used as lower gate electrodes.[38] Even though the thicknesses of both concave and trapezoidal shaped electrodes were more than 500 nm and 2.5 times thicker than the dielectric layers, the fabricated capacitors with shape-controlled lower electrodes exhibited excellent electrical breakdown strength.

Figure 4c shows the transfer characteristics of fabricated organic TFT devices with trapezoidal shaped gate electrodes. The gate-source voltage (V_{GS}) was swept from +10 to −20 V with source-drain voltage (V_{DS}) = −20 V. The source-drain current (I_{DS}) was found to be 15 μA at a relatively low operating voltage of −20 V, and the maximum gate leakage current (I_{GS}) was 20 pA even at V_{GS} = −20 V. The gate leakage current is smaller than the drain current by more than 6 orders of magnitude, confirming the high quality of the molecular gate dielectric. The field-effect mobility (μ) and threshold voltage (V_{TH}) of the transistors were calculated in the saturation

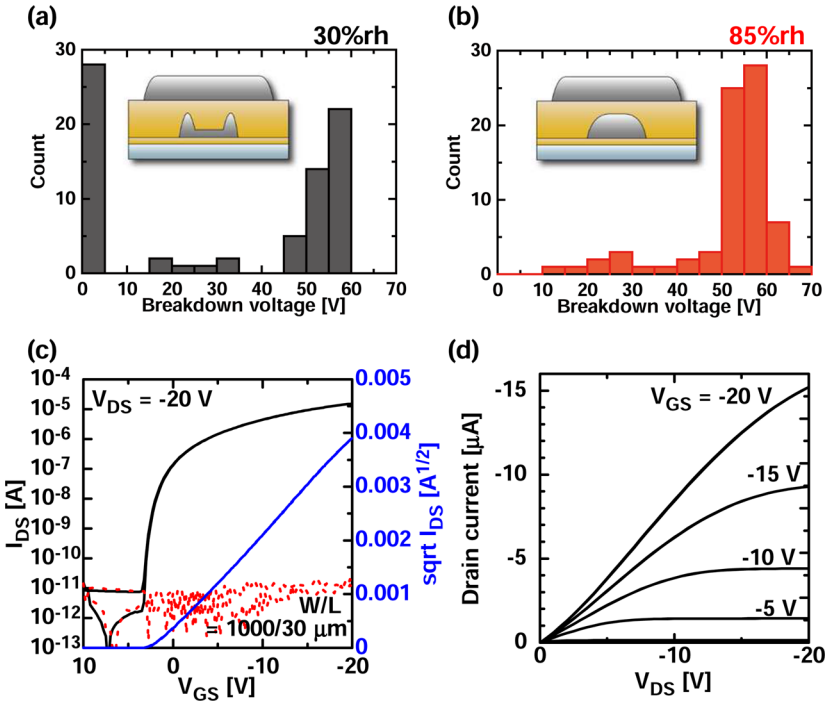

Figure 4. Breakdown voltage histograms for the fabricated capacitors with different drying conditions, at 30 °C, 30% RH for 30 min (a) and at 30 °C, 85% RH for 30 min (b). The total number of counts was 75 for each condition. (c) Transfer characteristics of fabricated organic TFT devices with shape-controlled lower gate electrodes. The TFT devices have a channel width/channel length (W/L) ratio of 33. The gate-source voltage (V_{GS}) was swept from +10 to −20 V with V_{DS} = −20 V. The solid black line represents the source-drain current (I_{DS}), and the dotted red line represents the gate leakage current (I_{GS}). (d) Output characteristics for the same device. The gate-source voltage (V_{GS}) was varied from 0 to −20 V in steps of −5 V.

regime, V_{DS} = −20 V from the equation which describes the source-drain current as a function of gate-source voltage:[39]

$$I_{DS} = \frac{\mu CW}{2L}(V_{GS} - V_{TH})^2 \quad (3)$$

Here, C is the capacitance per unit area of the gate dielectric layer, L is the channel length, and W is the channel width. The estimated field-effect mobility in the saturation region was 0.13 $cm^2/(V\ s)$, the threshold voltage was 1.0 V, and the on/off ratio was greater than 10^6, which is comparable to that of a pentacene TFT device formed using evaporated gold source/drain electrodes on treated SiO_2 substrates[40] and that were formed using printed silver source/drain electrodes with evaporated metal gate electrodes.[41]

Figure 4d shows the output characteristics for the same TFT device. Here, the drain current was measured as a function of V_{DS} at a V_{GS} between 0 and −20 V in steps of 5 V. Despite the fact that the gate dielectric layers were thinner than the gate electrodes, the fabricated dielectric layers have excellent insulating properties, which resulted in large on/off ratios. Furthermore, the fabricated TFT devices were operated at low operating voltages with reasonable field-effect mobility. In summary, controlling the shape of lower gate electrodes provides for the use of thinner dielectric layers and for organic TFT devices with low-operating voltages. These TFT results indicate that techniques for the controlling the shape of inkjet-printed silver electrodes can be applied to the printed electronics that have stacked layer constructions.

CONCLUSIONS

In this paper, we have reported on the effect of drying conditions on the cross-sectional profile of inkjet printed electrodes formed using silver nanoparticle inks with water-based solvents. High ambient humidity suppresses the solvent evaporation speed, whereby the film shape can be easily controlled from being concave to trapezoidal to convex by changing the ambient humidity level and drying time. The methods for controlling the shape of printed electrodes described in this paper do not require changes in ink formulation or in any of the printing process conditions, but only drying conditions after printing, and, as a result, can be utilized for not only inkjet printed electrodes, but also with other materials and alternate printing processes. Therefore, these methods increase freedom in printing conditions and could help in the practical realization of printed electronics.

AUTHOR INFORMATION

Corresponding Author

*E-mail: fukuda@yz.yamagata-u.ac.jp (K.F.). tokito@yz.yamagata-u.ac.jp (S.T.).

Notes

The authors declare no competing financial interest.

ACKNOWLEDGMENTS

We would like to acknowledge the Japan Science and Technology Agency (JST) for their support of this work. We also thank DIC Corporation for providing silver nanoparticle ink.

REFERENCES

(1) Calvert, P. *Chem. Mater.* **2001**, *13*, 3299−3305.
(2) Teichler, A.; Eckardt, R.; Hoeppener, S.; Friebe, C.; Perelaer, J.; Senes, A.; Morana, M.; Brabec, C. J.; Schubert, U. S. *Adv. Energy Mater.* **2011**, *1*, 105−114.

(3) Minemawari, H.; Yamada, T.; Matsui, H.; Tsutsumi, J.; Haas, S.; Chiba, R.; Kumai, K.; Hasegawa, T. *Nature* **2011**, *475*, 364−367.
(4) Torrisi, F.; Hasan, T.; Wu, W.; Sun, Z.; Lombardo, A.; Kulmala, T. S.; Hsieh, G.-W.; Jung, S.; Bonaccorso, F.; Paul, P. J.; Chu, D.; Ferrari, A. C. *ACS Nano* **2012**, *6*, 2992−3006.
(5) Caironi, M.; Gili, E.; Sakanoue, T.; Chen, X.; Sirringhaus, H. *ACS Nano* **2010**, *4*, 1451−1456.
(6) Ng, T. N.; Schwartz, D. E.; Lavery, L. L.; Whiting, G. L.; Russo, B.; Krusor, B.; Veres, J.; Bröms, P.; Herlogsson, L.; Alam, N.; Hagel, O.; Nilsson, J.; Karlsson, C. *Sci. Rep.* **2012**, *2*, 585.
(7) Jung, M.; Kim, J.; Noh, J.; Lim, N.; Lim, C.; Lee, G.; Kim, J.; Kang, H.; Jung, K.; Leonard, A. D.; Tour, J. M.; Cho, G. *IEEE Trans. Electron. Devices* **2010**, *57*, 571.
(8) Allen, M.; Lee, C.; Ahn, B.; Kololuoma, T.; Shin, K.; Ko, S. *Microelectron. Eng.* **2011**, *88*, 3293−3299.
(9) Maiwald, M.; Werner, C.; Zoellmer, V.; Busse, M. *Sens. Actuators, A.* **2010**, *162*, 198−201.
(10) Jang, J.; Ha, J.; Cho, J. *Adv. Mater.* **2007**, *19*, 1772−1775.
(11) Böberl, M.; Kovalenko, M. V.; Gamerith, S.; List, E. J. W.; Heiss, W. *Adv. Mater.* **2007**, *19*, 3574−3578.
(12) Deegan, R. D.; Bakajin, O.; Dupont, T. F.; Huber, G.; Nagel, S. R.; Witten, T. A. *Nature* **1997**, *389*, 827−829.
(13) Chung, S.; Kim, S. O.; Kwon, S.-K.; Lee, C.; Hong, Y. *IEEE Electron Device Lett.* **2011**, *32*, 1134−1136.
(14) Hambsch, M.; Reuter, K.; Stanel, M.; Schmidt, G.; Kempa, H.; Fügmann, U.; Hahn, U.; Hübler, A. C. *Mater. Sci. Eng., B* **2010**, *170*, 93−98.
(15) Kajiya, T.; Nishitani, E.; Yamaue, T.; Doi, M. *Phys. Rev. E* **2006**, *73*, 011601.
(16) Zhang, L.; Maheshwari, S.; Chang, H. C.; Zhu, Y. *Langmuir* **2008**, *24*, 3911−3917.
(17) Kim, D.; Jeong, S.; Park, B. K.; Moon, J. *Appl. Phys. Lett.* **2006**, *89*, 264101.
(18) Kajiya, T.; Kobayashi, W.; Okuzono, T.; Doi, M. *J. Phys. Chem. B* **2009**, *113*, 15460−15466.
(19) Still, T.; Yunker, P. J.; Yodh, A. G. *Langmuir* **2012**, *28*, 4984−4988.
(20) Kang, B. J.; Oh, J. H. *Thin Solid Films* **2010**, *518*, 2890−2896.
(21) Kim, J. H.; Park, S. B.; Kim, J. H.; Zin, W. −C. *J. Phys. Chem. C* **2011**, *115*, 15375−15383.
(22) Soltman, D.; Subramanian, V. *Langmuir* **2008**, *24*, 2224−2231.
(23) Kim, C.; Nogi, M.; Suganuma, K. *J. Micromech. Microeng.* **2012**, *22*, 035016.
(24) Kajiya, T.; Kobayashi, W.; Okuzono, T.; Doi, M. *Langmuir* **2010**, *26*, 10429−10432.
(25) Majumder, M.; Rendall, C. S.; Eukel, J. A.; Wang, J. Y. L.; Behabtu, N.; Pint, C. L.; Liu, T.-Y.; Orbaek, A. W.; Mirri, F.; Nam, J.; Barron, A. R.; Hauge, R. H.; Schmidt, H. K.; Pasquali, M. *J. Phys. Chem. B* **2012**, *116*, 6536−6542.
(26) Cui, L.; Zhang, J.; Zhang, X.; Huang, L.; Wang, Z.; Li, Y.; Gao, H.; Zhu, S.; Wang, T.; Yang, B. *ACS Appl. Mater. Interfaces* **2012**, *4*, 2775−2780.
(27) Yunker, P. J.; Still, T.; Lohr, M. A.; Yodh, A. G. *Nature* **2011**, *476*, 308−311.
(28) Ng, T. N.; Russo, B.; Krusor, B.; Kist, R.; Arias, A. C. *Org. Electron* **2011**, *12*, 2012−2018.
(29) Fuller, S. B.; Wilhelm, E. J.; Jacobson, J. M. J. *Microelectronmech. Syst.* **2002**, *11*, 54−60.
(30) Li, Y.; Wu, Y.; Ong, B. S. *J. Am. Chem. Soc.* **2005**, *127*, 3266−3267.
(31) Lee, H.-H.; Chou, K.-S.; Huang, K. -C. *Nanotechnology* **2005**, *16*, 2436−2441.
(32) Lee, D. J.; Oh, J. H.; Bae, H. S. *Mater. Lett.* **2010**, *64*, 1069−1072.
(33) Ashimine, T.; Yasudai, T.; Saito, M.; Nakamura, H.; Tsutsui, T. *Jpn. J. Appl. Phys.* **2008**, *47*, 1760−1762.
(34) Fukuda, K.; Yokota, T.; Kuribara, K.; Sekitani, T.; Zschieschang, U.; Klauk, H.; Someya, T. *Appl. Phys. Lett.* **2010**, *96*, 053302.
(35) Sobac, B.; Brutin, D. *Phys. Rev. E* **2012**, *86*, 021602.
(36) Hu, H.; Larson, R. G. *J. Phys. Chem. B* **2002**, *106*, 1334−1344.
(37) Okuzono, T.; Kobayashi, M.; Doi, M. *Phys. Rev. E* **2009**, *80*, 021603.
(38) Yoon, M.-H.; Yan, H.; Facchetti, A.; Marks, T. J. *J. Am. Chem. Soc.* **2005**, *127*, 10388−10395.
(39) Klauk, H. *Chem. Soc. Rev.* **2010**, *39*, 2643−2666.
(40) Pesavento, P. V.; Chesterfield, R. J.; Newman, C. R.; Frisbie, C. D. *J. Appl. Phys.* **2004**, *96*, 7312−7324.
(41) Fukuda, K.; Sekine, T.; Kobayashi, Y.; Takeda, Y.; Shimizu, M.; Yamashita, N.; Kumaki, D.; Itoh, M.; Nagaoka, M.; Toda, T.; Saito, S.; Kurihara, M.; Sakamoto, M.; Tokito, S. *Org. Electron.* **2012**, *13*, 3296−3301.